3D Hybrid Wound Devices for Spatiotemporally Controlled Release Kinetics

Ibrahim T. Ozbolat[1,2,*] and Bahattin Koc[3,4]

[1]*Mechanical and Industrial Engineering Department, The University of Iowa*
2130 Seamans Center, Iowa City, IA 52242, USA

[2]*Center for Computer-aided Design, The University of Iowa*
216 Engineering Research Facility, Iowa City, IA 52242, USA

[3]*Industrial and Systems Engineering Department, University at Buffalo (SUNY)*
438 Bell Hall, Buffalo, NY 14260, USA

[4]*Faculty of Engineering and Natural Sciences, Sabanci University, FENS G013*
Orhanli-Tuzla, Istanbul, 34956, Turkey

ABSTRACT

This paper presents localized and temporal control of release kinetics over 3-dimensional (3D) hybrid wound devices to improve wound healing process. Imaging study is performed to extract wound bed geometry in 3D. Non-Uniform Rational B-Splines (NURBS) based surface lofting is applied to generate functionally graded regions. Diffusion-based release kinetics model is developed to predict time-based release of loaded modifiers for functionally graded regions. Multi-chamber single nozzle solid freeform dispensing system is used to fabricate wound devices with controlled dispensing concentration. Spatiotemporal control of biological modifiers thus enables a way to achieve target delivery to improve wound healing.

Keywords: Wound healing, Release Kinetics, Hybrid Wound Devices

Corresponding Author: Ibrahim T. Ozbolat

2130 Seamans Center, University of Iowa, Iowa City, 52242, IA, USA

Tel: (319) 384 0810 Fax: (319) 335 5669

ibrahim-ozbolat@uiowa.edu

1 INTRODUCTION

Loss of skin integrity due to injuries or serious illness may bring disabilities or even death. Main causes of significant skin loss are thermal injuries with around 1 million yearly emergency room visits, traumas (35 million wounds/yr in the United States) and chronic ulcerations [1]. Approximately 2 million cases of chronic ulceration are diagnosed every year. Due to possible lack of synchrony in the order of healing process, a chronic wound may fail to heal.

Despite extensive research, wound healing remains partially understood. Human skin serves as a protective barrier against the environment and is composed of two layers: keratinized stratified outer layer (epidermis) and collagen-rich inner layer (dermis) [2]. Serious injuries or illnesses damage the epidermis and sometimes even penetrates through the dermis. Wound contraction and matrix remodeling occur in the dermis in parallel with epidermal cell migration and proliferation during deep wound healing. In the literature, wound healing of mammalian skins has been analyzed both experimentally and theoretically [3-7]. Several mathematical models have been proposed concentrating specifically upon the mechanism involved in epidermal healing. However, 3-D healing modeling of deep wounds and closure has not been investigated, and majority of research has been done by assuming a 1-D or 2-D healing process. Wound closure is indeed the centripetal movement process of the wound periphery and adjacent uninjured skin toward the wound center [8]. The healing of convex wound shapes follows a linear relationship between area and perimeter while the distance from the wound perimeter to any given point within the wound surface is always definable via a linear distance [4]. Moreover, several imaging techniques such as Laser Doppler Imaging [9], noninvestment tools with magnetic resonance imaging (MRI) [10] and 3D active contour segmentation [11] are used to capture wound geometry during healing process, and predict wound healing based on geometry, area and appearance [12-15].

Biomaterials have been extensively used in medical applications. Alginates have been widely applied as hydrogel synthetic extracellular matrices (ECMs) for cell immobilization, cell transplantation and tissue engineering due to their physical properties that are similar to natural tissues [16]. Due to their

gelatin property during in contact with body fluid, alginates have been one of the most popular

biomaterials in wound care [17]. This property prevents the wound surface from drying out and provides

a moist wound environment that leads a better repair of wound with less tissue loss from desiccation [18].

Besides, this eliminates fibre entrapment in the wound, which is a major cause of patient trauma during

wound dressing removal [19]. Moreover, ionically crosslinked alginates release ions during in contact

with body fluids that reduce bleeding during several surgical interventions [20]. Furthermore, alginate is

highly absorbent (up to 15-20 times its own weight) and nonadherent that enables it to remain in wound

bed for several days [21]. Several biological modifiers (i.e. growth factors and proteins) are used to

enhance quantity and quality of regenerating skin tissue depending on their activity with target cells and

the extracellular matrix environment [3]. A wealth of growth factors such as epidermal growth factors

(EGF), platelet-derived growth factor (PDGF) and keratinocyte growth factor (KGF) regulate wound

healing [4]. Release of these modifiers with spatial and temporal gradient concentration mediates tissue

regeneration process [22]. It develops a mental biology, in which cells are guided by a mechanism with

respect to obtained spatial and directional cues [23]. As a result, wound dressings in tissue engineering

should be developed in way that they enable controlled release scheme of biological modifiers with

distinct spatial gradient to guide specific cues to the cellular microenvironment. Wound healing can be

enhanced by controlling localized protein and growth factor release. Adjusting the healing time of a

specific region with respect to the release time of corresponding growth factors or proteins would have a

great impact on wound healing [24]. Target delivery of biological modifiers at a specific site over the

wound space can be enabled by synchronizing the delivery of controlled amount of biological modifiers

with tissue regeneration.

In the literature, tremendous efforts have been made to analyze the use of protein and growth factors

for improving chronic or delayed skin wound closure [25, 26]. MacKay and Miller [27] studied effects of

nutritional and botanical support on wound healing process and concluded that adequate protein intake is

necessary for proper wound healing otherwise; depletion of protein delays wound healing and inhibits

3

wound remodeling. Choate and Khavari [28] showed that the bioactivity of proteins and growth factors is difficult to maintain in the wound space due to protein instability in protein-rich regions or resulting side effects when applied growth factor amount is high, and Putney and Burke [24] necessitated the spatial and temporary control of protein and growth factors in a wound device due to their short biological half-life, potential carcinogenesis risk and lack of tissue selectivity. Proteins can denature under a variety of circumstances such as changes in temperature, pH and hydrophobic environments [29].

In this paper, cells, proteins, growth factors, drugs and surfactants, which can control cellular environment and tissue regeneration, and be delivered by means of microspheres, are named with a general term "biological modifiers". Development of 3D engineered wound devices with superior control over cell-biological modifier interactions is still very much infancy. Advancing through heterogeneous multifold wound dressings with controlled release fashion enables synchronization of regenerating tissue with the release kinetics of loaded biological modifiers. This might be an engineering challenge and promising approach for improved and efficient tissue regeneration. The most critical limitations: the selection of proper biological modifier(s) incorporation, precise control over concentration gradient and timing should be overcome. Hence, wound devices need to be designed, modeled and fabricated in a way that biological modifiers should be incorporated and released in a specific spatial and temporal orientation to mimic the natural wound healing process. The goal of this paper is to develop a framework that enables design, modeling and fabrication of 3D hybrid wound devices for spatiotemporal control of biomaterial and loaded biological modifier composition.

2   MATERIALS AND METHODS

2.1   Materials

Alcian blue, sodium alginate from brown algae and calcium chloride were purchased from Sigma-Aldrich. Micro-glass beads in powder form were purchased from Corpuscular Inc. Nozzle tips for dispensing systems were purchased from EFD®.

2.2 Preparation and Fabrication of Alginate Wound Dressings

Alginate solutions with 3.5% and 4.5% (w/v) concentrations were prepared by suspending sodium alginate (SA) into DI water. Micro-glass beads in 0.36% and 0.54% (w/v) concentration were mixed in 3.5% and 4.5% (w/v) alginate solutions, respectively. Calcium chloride was suspended in DI water to obtain 0.6% (w/v) calcium chloride solution. Then SA/bead/DIwater solutions were stirred for 30min in room temperature to get even distribution. Biofabrication of wound devices is performed by using a multi-chamber single nozzle dispensing system. Fabrication process is biologically compatible. The system runs in room temperature under low pressure (0-5 psi) to reduce fluidic shear forces that can damage incorporated modifiers or diminish their active properties. The dispensing system is driven by a FlashCut CNC 3D motion controller. A PC is connected to the system to control the motion in 3D. Toolpath for the motion is realized through importing CAD models in stereolithography (STL) format followed by G-code generation using visual basic-based in-house developed script. The multi-chamber single nozzle assembly is mounted on the 3D motion control unit. The multi-chamber single nozzle assembly consists of multiple biomaterial chambers and a single converging nozzle unit, where two different biomaterials can be mixed statically and extruded with unique properties. The volume of the static mixture nozzle is optimized while nozzle volume determines the quality and the evenness of physical properties of the dispensed biomaterial. Biomaterial chambers are connected to a pressure control unit (Nordson EFD), where the air pressure assists in extruding the biomaterial through the dispensing unit. Material flow and concentration through the nozzle is controlled by regulating positive chamber pressures connected to the air pressure control unit. Mixing two different concentrations from each chamber enables dispensing varying concentration of alginate and loaded microspheres by time. Final solutions were deposited through 250 μm nozzle tip. The system allows extrusion of continuous customized filaments with variational biomaterial and biological modifier properties enabling controlled release kinetics. Calcium chloride solution is then dispensed onto printed alginate structure through another nozzle to provide crosslinking between the alginate anion and the calcium cation. Dark field

5

images of fabricated samples are taken by 5.0x1.0x1.0 optic lenses. The reader is referred to our earlier work [30] for further details of the dispensing system.

2.3   Wound Bed Surface Construction

Digital full thickness wound images are used to generate 3D wound bed geometry using Image J software 3D plug-in. Pixel values obtained from the digital image are converted into point cloud in CAD. Noise in point clouds is removed. 3D NURBS surface is then fitted to point cloud in Rhinoceros 4.0 software [31]. Constructed NURBS surface in this section is defined as the external surface of the developed wound device.

2.4   Geometric Modeling: Functionally Graded Region Generation

3D NURBS surface constructed in Section 2.3 is used to create functionally graded regions. The aim of this section is to discretize wound device geometry into a number of regions with various biomaterial and modifier concentration. Discretization of the device should follow how a wound heals on human skin. In order to mimic 3-D wound healing process to partition the wound device into uniform functional regions, concentration variation can be represented with relation to the 3D wound space boundaries. Mimicking natural healing process is desirable for the discretization procedure. In this study, we propose 3D lofting based wound healing process, in which a wound bed surface is morphed and converged into a final healing point. Based on our earlier work [32], final healing point can be approximated as the projection of deepest wound bed surface onto the top surface of the wound. Hence, parametric discretization is performed from wound bed surface to the final healing point. Release kinetics of modifiers can be temporarily controlled by controlling biomaterial and loaded modifier distribution spatially. Thus, 3D geometry of customized device is formed by partitioning the device geometry into uniform regions with uniform existence of biomaterials and modifiers. In this section, 3D lofting procedure is presented to mimic natural wound healing process. The wound bed surface $S_o(u,v)$ of the wounded volume can be defines as a NURBS surface:

6

$$S_o(u,v) = \frac{\sum\limits_{i=0}^{I}\sum\limits_{j=0}^{J} N_{i,p}(u)N_{j,q}(v)w_{i,j}P_{i,j}}{\sum\limits_{i=0}^{I}\sum\limits_{j=0}^{J} N_{i,p}(u)N_{j,q}(v)} \qquad (1)$$

where $P_{i,j}$ are the control points of the wound surface and $w_{i,j}$ are the weights of each $P_{i,j}$. $N_{i,p}(u)$ and

$N_{j,q}(v)$ are the B-spline basis functions defined on the knot vectors, **U** and **V**, with degree p and q,
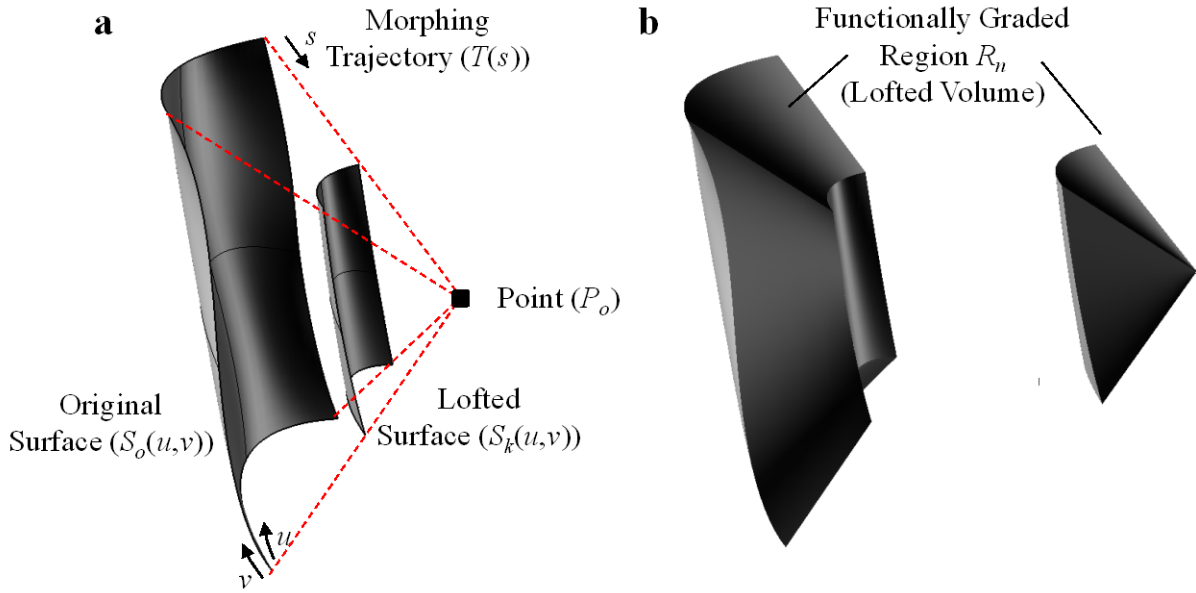
respectively.

Figure 1: Morphing process: (a) lofted surface generation and (b) construction of lofted volume.

Figure 1(a) illustrates a morphing process, in which a NURBS surface ($S_o(u,v)$) morphs into a point P_o.

Morphing proceeds through morphing trajectory ($T(s)$), in which $T(s)$ is defined as a linear

correspondence between $S_o(u,v)$ and P_o [33]:

$$T(s) = \frac{\sum\limits_{m=0}^{M} N_{m,t}(s)w_m C_m}{\sum\limits_{m=0}^{M} N_{m,t}(s)} \qquad (2)$$

7

In Equation (2), C_m are the control points of the trajectory and w_m are the weights of each C_m. $N_{m,t}(s)$ is the B-spline basis function defined on the knot vector **S** with degree t. By combining Equation (2) and (3), interpolation between $S_o(u,v)$ and P_o along the trajectory $T(s)$ gives the functionally graded regions R_n, which defines the lofted volume as below:

$$R_n(u,v,s) = \frac{\sum_{i=0}^{I}\sum_{j=0}^{J}\sum_{m=0}^{M} N_{i,p}(u)N_{j,q}(v)N_{m,t}(s)w_{i,j,m}P_{i,j,m}}{\sum_{i=0}^{I}\sum_{j=0}^{J}\sum_{m=0}^{M} N_{i,p}(u)N_{j,q}(v)N_{m,t}(s)} \tag{3}$$

where $P_{i,j,m}$ are the control points of the lofted volume and $w_{i,j,m}$ are the weights of each $P_{i,j,m}$. $N_{i,p}(u)$, $N_{j,q}(v)$ and $N_{m,t}(s)$ are the B-spline basis functions defined on the knot vectors, **U**, **V**, **S** with degree p, q, t, respectively. Lofted volumes generated in Figure 2(b) stand as functionally graded regions, in which different biomaterial and biological modifier composition can be assigned.

2.5   Construction of Hybrid Devices

Solid freeform fabrication (SFF) has been widely used for constructing tissue engineered devices due to its high accuracy in micro-scale fabrication resolution [34, 35]. Applied SFF technology is recently utilized in drug metabolism studies and direct cell printing process for layer-by-layer dispensing of 3D alginate tissue scaffolds [36, 37]. In order to achieve truly interconnected internal architecture for cell growth and proliferation, the device is formed by depositing cylindrical micro-filaments parallel to each other in every layer using a certain lay-down pattern. In this research, a visual basic script was developed in Rhinoceros software to prepare fabrication process plan for hybrid device development. Firstly, lofted volumes are uniformly sliced where multiple contours are generated on each slice. The slice thickness is set to be equal to filament thickness. Next, corresponding filament properties including biomaterial and biomolecule concentrations are assigned to each region on each slice. Horizontal deposition over each slice is then started with generating a number of equidistance horizontal lines, where intersection of these

8

horizontal lines with the contours are defined as starting and ending points of filament deposition. Then, toolpath is generated through tracing each slice by adding straight filaments in lay-down pattern along equidistance lines with orientation direction 0°/90°. During straight filament deposition, composition of a filament changes when the filament enters a new functionally gradient region and new concentration values are assigned based on the concentration profile of each region, which is assumed to follow tissue engineering needs. All the information including starting and ending points of filament deposition on each slice, region based biomaterial and biomolecule concentration values as well as points where the region change is observed is printed in a G-code file to control 3D motion and the pressure levels for each biomaterial chamber. The code is then imported into the control unit to fabricate porous heterogeneous medical devices, in which overall composition changes along functionally gradient direction.

2.6   Release Kinetics through Sodium Alginate Filaments

While hybrid alginate devices have functionally graded regions with different biomaterial concentration, media penetration and hence biological modifier transport through the biomaterial mesh structure shows variability over the geometry. This necessitates determination of diffusion characteristics for each region. Data for solute diffusion in pure water D_{aq} is extensively available in the literature [38]. The effective diffusion constant D_{eff} for polymeric device can be then determined using the following relation [39]:

$$D_{eff} = D_{aq} \frac{(1-Q)^3}{(1+Q)^2} \tag{4}$$

Q in Equation (4) stands for the volume fraction of alginate in swollen state and can be found using the following relation discussed in [40]:

$$Q = \left[1 + \left(\frac{p_{polymer}}{p_{solvent}}\right)\left(\frac{M_a}{M_b} - 1\right)\right]^{-1} \tag{5}$$

Where $p_{polymer}$ and $p_{solvent}$ are the densities of polymer and solvent, and M_a and M_b are the weight of the polymer after and before swelling, respectively. Although experimental swelling study has been

conducted for cylindrical alginate slabs where height (L) and diameter (d) are equal [41], a correction procedure is presented in Appendix A to determine the volume fraction of the alginate for cylindrical filaments ($L>>d$), while the device is constructed from laydown pattern of cylindrical alginate filaments.

Penetration of media through alginate network is mediated by diffusion process. Diffusion of media through a cylindrical polymeric domain is modeled using Fick's second law as in Equation (6), where D is the diffusion coefficient, C is the media concentration at time t and r, q and z denote radial, angular and axial directions, respectively.

$$\frac{\partial C}{\partial t} = \frac{1}{r}\left[\frac{\partial}{\partial r}\left(rD\frac{\partial C}{\partial r}\right) + \frac{\partial}{\partial \theta}\left(\frac{D}{r}\frac{\partial C}{\partial \theta}\right) + \frac{\partial}{\partial z}\left(rD\frac{\partial C}{\partial z}\right)\right] \tag{6}$$

For cylindrical geometries with aspect ratios $(L >> d)$, it has been shown that edge effects could be negligible [42]. Moreover, there is no concentration gradient of any of the three components with respect to q. By ignoring diffusion through angular and axial directions, Equation (6) can be simplified into Equation (7):

$$\frac{\partial C}{\partial t} = D\left[\frac{\partial^2 C}{\partial r^2} + \frac{1}{r}\frac{\partial C}{\partial r}\right] \tag{7}$$

The solution of Equation (7) can be derived as in Equation (8) and experimentally validated in [39]:

$$\frac{M_t}{M_\infty} = 1 - \frac{8}{h^2 r^2}\sum_{m=1}^{\infty}\alpha_m^{-2}\exp(-D\alpha_m^2 t)\sum_{n=0}^{\infty}\beta_n^{-2}\exp(-D\beta_n^2 t) \tag{8}$$

Where h denotes the half length of the filament and r is the radius of the filament. a and b can be obtained by solving Equations (9)-(10). In Equation (8), m and n are integers and a stands for the root of a zero-order Bessel function J_0.

$$J_0(r\alpha) = \sum_{k=0}^{\infty}\frac{(-1)^k\left(\frac{r\alpha}{2}\right)^{2k}}{k!\,\Gamma(k+1)} = 0 \tag{9}$$

$$\beta_n = \frac{(2n+1)\pi}{2h} \tag{10}$$

Following approximation can be proposed for roots of a zero-order Bessel function when $m > 10$:

$$\alpha_m : \alpha_m \cong \alpha_{m-1} + \pi \quad \forall m > 10 \tag{11}$$

Thus, Equations (8)-(11) can be used to determine the time based released kinetics through alginate filaments. Next section presents results and discussions.

3   RESULTS AND DISCUSSIONS

For implementation purposes, a digital image of a full thickness chronic wound [43] is used (Figure 2(a)). The digital image is processed in ImageJ software to extract 3D model of the wound bed surface as shown in Figure 2(b). Then, pixel points of the wound bed are transformed into 3D point cloud in CAD. Next, noise is eliminated and a 3rd degree NURBS B-spline surface is fitted in Rhinoceros 4.0. Generated 3D B-spline surface is presented in Figure 2(c).
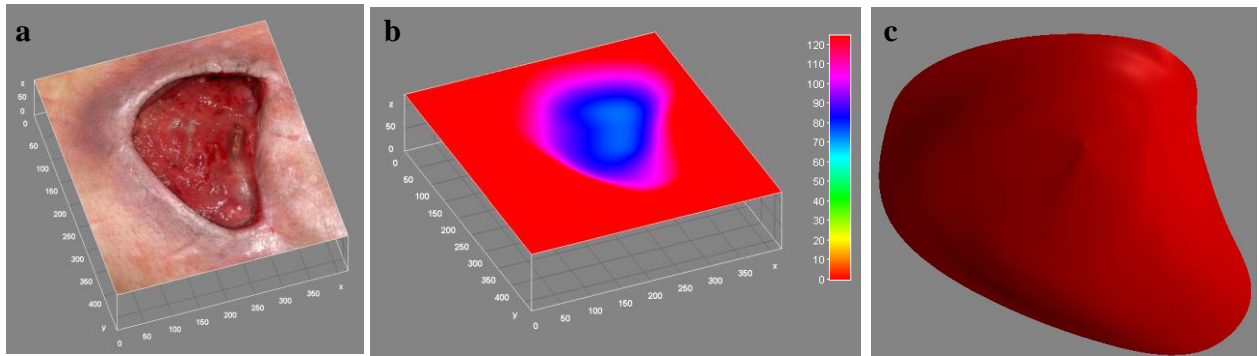
Figure 2: (a) A chronic wound image [43] from the literature is processed (b) using ImageJ software and (c) 3D NURBS surface is obtained in Rhinoceros.

Based on linear wound healing fashion as discussed in the introduction section, 3D lofting is used to generate lofted surfaces as equal parameter distances between the wound surface and final healing point. Interpolation is performed between wound bed surface and final healing point as presented in Figure 3(a) and lofted surfaces $\mathbf{S} = \{S_k(u,v)\}_{k=1,\dots,K}$ are obtained at equal parametric distances from the wound bed surface. Layer-by-layer manufacturing methodology is used to build 3D model in CAD (See Figure 3(c)). Functionally graded regions are then generated using lofted surfaces as boundaries using our earlier work

11

[30]. Figure 3(d) illustrates a 3D porous hybrid wound device highlighting functionally graded regions, where the wound device is portioned into 4 regions: Regions 1-4.
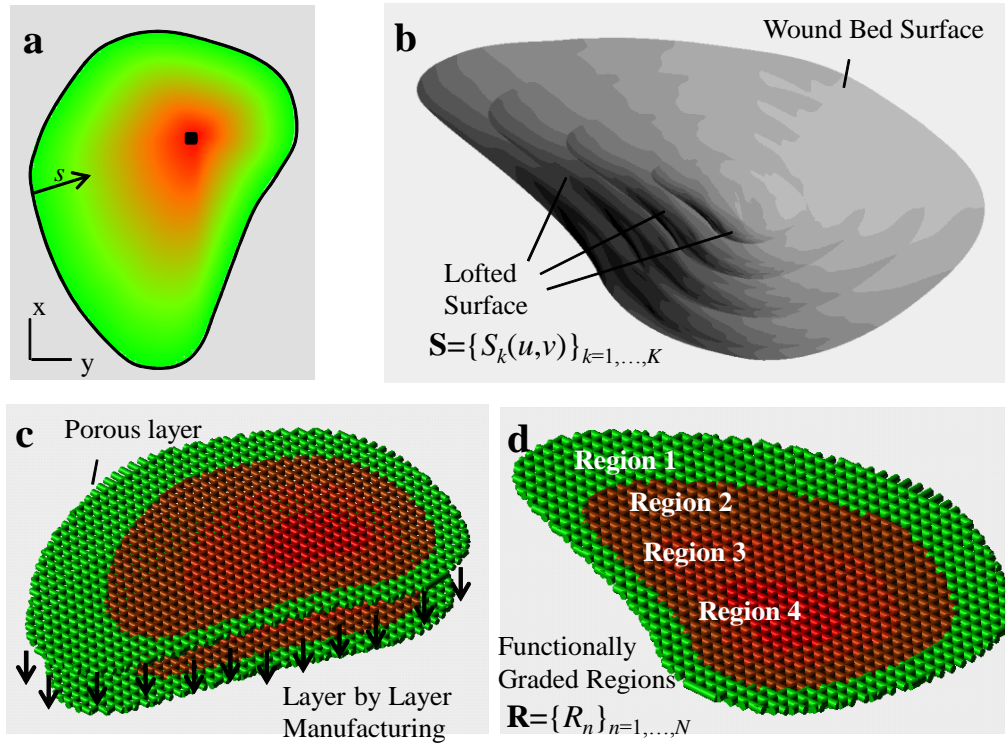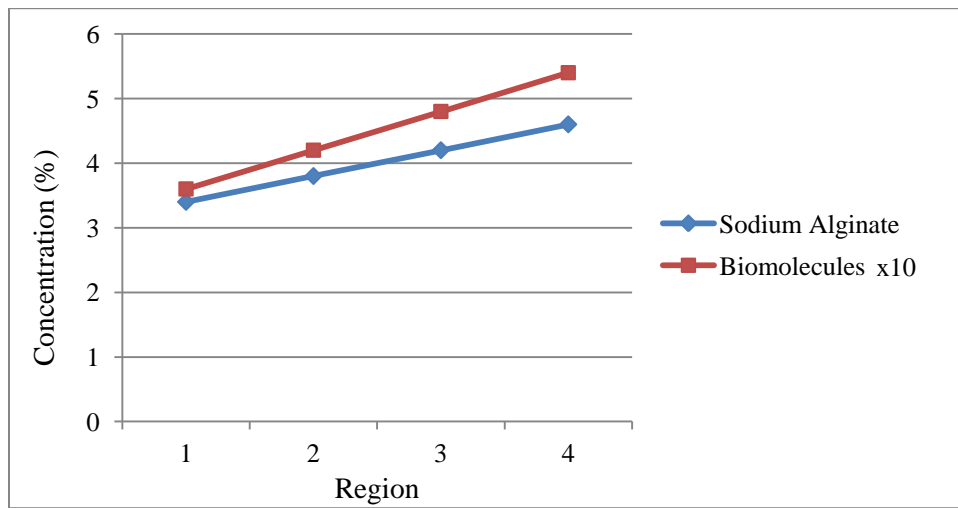

Figure 3: (a) Linear wound healing fashion from wound bed surface to final healing point, (b) generation of lofted surface, and (c) a 3D hybrid wound device with functionally graded regions.

In the next step, biomaterial and modifier concentration is determined according to tissue engineering requirements. There are several criteria to determine the loading concentrations such as viability condition of cells at different biomaterial concentrations, natural wound healing process, optimum biological modifier amount etc. Based on these requirements, loading of biomaterials and modifiers can be determined and release kinetics can be arranged accordingly.

Figure 4 shows concentration level of sodium alginate and biomolecules in Regions 1-4 on the wound device illustrated in Figure 3(d). Requirements presented in Figure 4 are assumed to be tissue engineering needs. In general, alginate concentration over 5% is not suitable for cell viability and concentration under 1% does not provide good mechanical integrity [41]. Thus, alginate concentration is preferred to be in the

range of 3% to 5%. Moreover, modifier concentration under 1% is in biologically relevant range [44]. Then, the concentration information is inputted into the fabrication system. A double layer of CAD model is printed through the deposition system with blending of two different alginate and modifier concentrations. Yellow and red inks in RGB are used for each alginate solutions to represent regional differentiation for visualization purposes. Only top layer is printed due to diffusive characteristics of color inks. The reader is referred to our earlier works for complex 3D fabrication on tissue replacement structures [45].

Figure 4: Concentration of sodium alginate and biomolecules

Based on requirements in Figure 4, a sample structure is printed in which the alginate concentration increases through the innermost region (Region 4). Figure 5 shows a sample fabricated wound dressing with 4 regions, in which regions are occupied by different alginate and modifier concentration based on the profile presented in Figure 4.
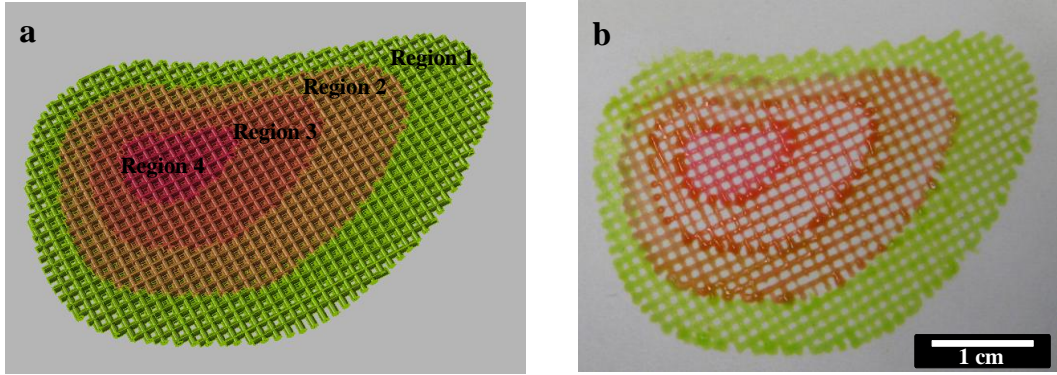
Figure 5: (a) Designed model in CAD and (b) fabricated wound device using multi-chamber single nozzle deposition system through 250μm nozzle tip.

A random region from printed sample is analyzed and a dark field image is taken by a 5.0x1.0x1.0 optic lenses. Loaded modifiers are highlighted in Figure 6. Different regions encapsulate different concentration of modifiers (UNIF (3-15 µm) in diameter). Using the experimental studies regarding the swelling characteristics of cylindrical alginate slabs at different concentration values from the literature [41] and applying the correction procedure to scale the swelling characteristics to a cylindrical filament given in Appendix A, swelling properties of alginate for various concentration ranges is obtained as in Table 1. As depicted in Table 1, volume fraction and density of alginate increases in the swollen state as alginate concentration increases. This can be explained by diminishing average mesh network opening size of alginate.
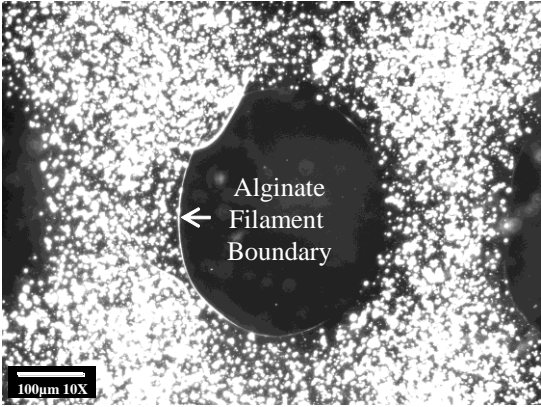

Figure 6: Dark field image of encapsulated modifiers (beads) with a uniform size distribution of 3-15 µm using 5.0x1.0x1.0 optic lenses.

Table 1: Characterization of diffusion coefficient at different alginate concentrations

Alginate Concentration (%)	M_a/M_b (Slab)	M_a/M_b (filament)	$p_{polymer}$ (g/mL)	$p_{solvent}$ (g/mL)	Q
1	73	16.576	1.01	1	0.060
1.5	56	13.750	1.015	1	0.072
2	42	11.209	1.02	1	0.088
3	30	8.795	1.03	1	0.111

In this work, effect of alginate concentration change over the release kinetics is analytically determined using Equations (8)-(11). For sake of demonstration, release kinetics of insulin is analyzed while it's treatment is critical in chronic diabetic wounds [46]. Using the polymer fraction Q and the diffusion constant of insulin in pure aqueous solution $D_{aq}=10^{-12}$ m^2/s [47], effective diffusion constant at different alginate concentrations is obtained and demonstrated in Figure 7. As can be depicted from the figure, diffusion coefficient decreases as the alginate concentration increases. This can be explained by the difficulty of media penetration with decrease in average network mesh opening diameter due to increased alginate concentration.
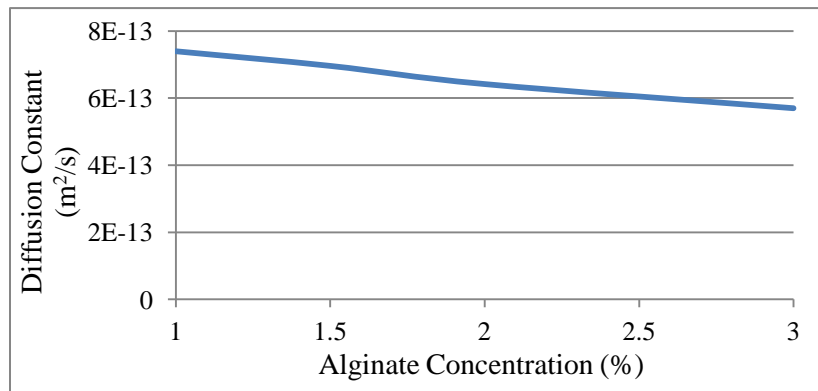

Figure 7: Diffusion coefficient of insulin through alginate network at different concentrations

Release kinetics of insulin is analyzed analytically through 250µm alginate filament under various concentration values using the developed methodology in Section 2.6 (See Figure 8). As the concentration of alginate increases, release kinetics slows down. Release of loaded insulin initializes with burst release and more than half of the protein releases within the first 2 hours. All concentration levels follow similar

release fashion starting with a burst release and continuing with decreasing rate of release kinetics. Release of insulin through 1% alginate concentration begins with 57% burst release in 2 hours and finalizes around 18h. Release of insulin through 1.5% alginate concentration however starts with 55% burst release and is completed in 24h. Increasing alginate concentration to 2% reduces the burst release and reduces the burst release to 53% at time 2h, in which release of insulin stops at 28h. The slowest release kinetics is attained at 3% alginate concentration in which 50% burst release is observed in 2h and release of insulin finalizes at 32h, which is almost double of total release time of insulin in 1% alginate concentration. As a result, change in concentration affects the release kinetics. Increasing alginate concentration slows down the release fashion.
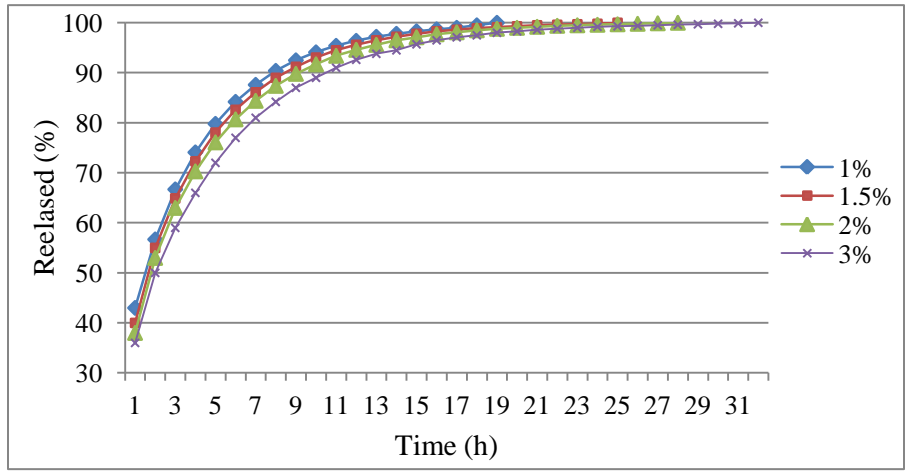
Figure 8: Insulin release through 250μm diameter micro-filaments for 4 different alginate concentrations

Based on Equation (8)-(11), increase in filament diameter also brings deceleration in release kinetics that can be explained by the increased diffusion distance of biomolecules through the filament. Figure 9 shows release kinetics profile for 250μm, 375μm and 500μm diameter micro-filaments at 2.5% alginate concentration. Increasing the filament diameter alleviates burst release and slows down the overall release fashion.
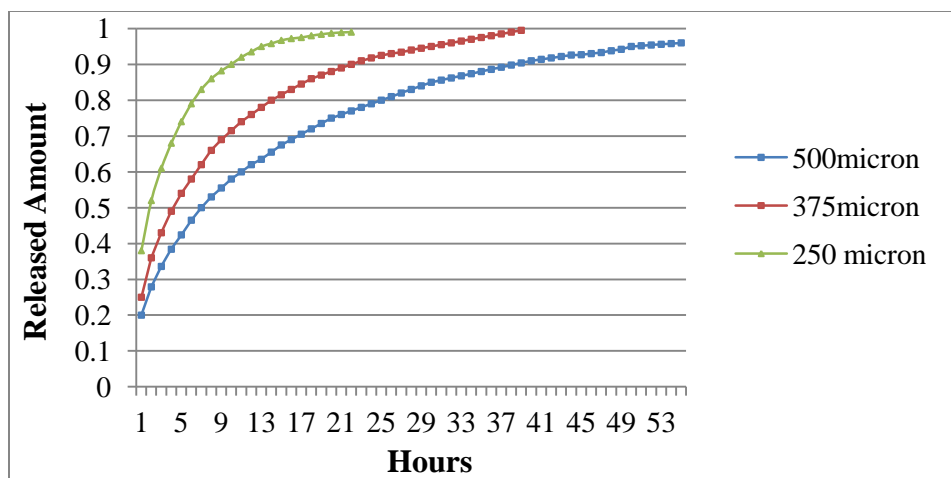
Figure 9: Insulin release through 250μm, 375μm and 500μm diameter micro-filaments for 2.5% alginate concentration.

In this paper, concentration of alginate increases through the innermost region so that release of loaded modifiers decelerates through innermost region that can enable synchronization of wound healing with the release kinetics. In order to lessen the effect of burst release and adjust the release time in a way that it can be synchronized with the healing wound, drugs can be loaded inside microspheres rather than directly loaded inside the alginate filament. This also delays the total release time of loaded biomolecules. For instance, loading insulin inside polymeric microspheres delays the release time significantly. The other important factor during biological modifier release is hydrodynamic resistance. Polymer chains in alginates are considered as centers of hydrodynamic resistance. During protein diffusion throughout the alginates network, polymer chains slow down the protein transport especially in sites nearby cross-links. Transport behavior of proteins in alginates can thus be explained by reduction in alginate free volume, increased hydrodynamic drag and path length due to abstraction. Furthermore, proteins can cluster around polymer chains forming biomass. Due to the formation of biomass (also called biofouling), protein transport is limited further and reduced or incomplete release is observable. This can diminish bioavailability of the therapeutic agent and alters overall delivery profile as well [48]. Alginate polymer network, crosslinking chemistry, polymer size, protein type and size, encapsulating material, its thickness

17

and size, and surfactant type all play role in release kinetics of loaded proteins through alginate network [49-55].

4 CONCLUSION

In this paper, we propose a new hybrid wound device to control release kinetics spatiotemporally to enhance wound healing process. Spatial and temporal control in this work enables synchronization of wound healing with the release kinetics to advance cell proliferation and tissue healing. Spatiotemporal control of release kinetics is achieved by controlling the distribution of base biomaterial and loaded biological modifiers. The proposed release model reveals different release characteristics along functionally gradient variation direction.

Transition from incorporation of a single modifier to multiple modifiers for wound care applications might be an engineering challenge and promising approach for improved and efficient tissue regeneration. As a future direction, wound devices needs to be designed and fabricated in a way that multiple proteins or growth factors should be impregnated and released in a specific spatial and temporal orientation to mimic the natural wound healing process. The authors are aiming at incorporating multiple proteins using the same bioprinting system to guide multiple clues in cell proliferation.

APPENDIX A

Experimental study conducted in [41] reveals the swelling properties of cylindrical sodium alginate slabs with a size of 6mm in radius and 6mm in height; however, this data cannot be applied directly while deposited filaments with 250µm in diameter follows a different swelling mechanism. While length of deposited filaments is significantly large compared to the radius, axial expansion can be ignored. Swelling

18

study of cylindrical hydrogel slabs in [56] showed that radial and axial expansions are closed to each other. Thus corrected values of the swelling ratio can be obtained through the following scheme. Volume of the polymer or dried alginate V_p can be represented as in the following formula:

$$V_{polymer} = \frac{M_{polymer}}{\rho_{polymer}} = \pi R^3 \tag{A.1}$$

Here $M_{polymer}$ and $\rho_{polymer}$ are the weight and density of the polymer, respectively. R is the filament radius which is equal to the height value. Expansion in radial and axial directions (ΔR) is same and weight of solvent in the swollen state can be calculated as in Equation (A.2), where $M_{solvent}$, $\rho_{solvent}$ and $V_{solvent}$ are the weight, the volume and the density of the solvent, respectively.

$$V_{solvent} = \frac{M_{solvent}}{\rho_{solvent}} = \pi(R + \Delta R)^3 - V_{polymer} = \pi(R + \Delta R)^3 - \pi R^3 \tag{A.2}$$

Swelling of a micro-filament however does not account for the expansion in axial direction while axial diffusion can be ignored with the filament length which is more than 10 fold greater than it's diameter [42]. Thus, corrected volume ($V_{solvent}^*$) and weight of the solvent ($M_{solvent}^*$) without axial expansion can be represented as:

$$V_{solvent}^* = \frac{M_{solvent}^*}{\rho_{solvent}} = R\left(\pi(R + \Delta R)^2 - \pi R^2\right) \tag{A.3}$$

By rearranging Equations (A.1)-(A-3), corrected mass can be derived as in Equation (A.4), where $\frac{M_a}{M_b}$ is the swelling ratio obtained from the experimental study in [41]:

$$M_{solvent}^* = M_{polymer}\left|\left(\frac{1}{\rho_{polymer}}\right)^{\frac{1}{3}}\left(\frac{\left[\frac{M_a}{M_b}\right]}{\rho_{solvent}} + \frac{1}{\rho_{polymer}}\right)^{\frac{2}{3}} - \frac{1}{\rho_{polymer}}\right| \tag{A.4}$$

Corrected swelling ratio thus can be used to calculate the polymer fraction ratio in Equation (5) to find the effective diffusion constant at different alginate concentrations.

19

REFERENCES

[1]   R. Lanza, R. Langer, and J. Vacanti, *Principles of Tissue Engineering*. 3 ed2007: Elsevier.

[2]   C. Pereira, W. Gold, and D. Herndon, Review Paper: Burn Coverage Technologies: Current Concepts and Future Directions, Journal of Biomaterials Applications 22 (2007) 101-121.

[3]   R. T. Tranquillo and J. D. Murray, Mechanistic Model of Wound Contraction, Journal of Surgical Research 55 (1993) 233-247.

[4]   M. Cardinal, D. E. Eisenbud, and D. G. Amstrong, Wound shape geometry measurement predict eventual wound healing, in 18th Annual Meeting of Wound Healing Society2008: San Diego, CA.

[5]   A. E. Savakis and S. A. Maggelakis, Models of Shrinking Clusters with Applications to Epidermal Wound Healing, Mathl. Comput. Modelin 25 (1997) 1-6.

[6]   G. J. Pettet, et al., A Model of Wound Healing Angiogenesis in Soft Tissue, Mathematical Biosciences 136 (1995) 35-63.

[7]   A. Manios, et al., Computer assisted evaluation of wound healing in chronic ulcers, Computers in Biology and Medicine 33 (2003) 311-317.

[8]   H. Sheardown and Y.-L. Cheng, Mechanism of Corneal Epithelial Wound Healing, Chemical Engineering Science 51(19) (1995) 4517-4529.

[9]   F. W. H. Kloppenberg, G. I. J. M. Beerthuizen, and H. J. t. Duis, Perfusion of burn wounds assessed by Laser Doppler Imaging is related to burn depth and healing time, Burns 27 (2001) 359-363.

[10]   T. H. Helbich, et al., Noninvasive Assessment of Wound-healing Angiogenesis with Contrast-enhanced MRI1, Acad Radiol 9(suppl 1) (2002) S145-S147.

[11]   P. A. Yushkevich, et al., User-guided 3D active contour segmentation of anatomical structures: Significantly improved efficiency and reliability, NeuroImage 31 (2006) 1116-1128.

[12]   M. Herbin, et al., Assessment of healing kinetics through true color image processing, IEEE Trans Med Imaging 12(1) (1993) 39-43.

[13]   F. X. Bon, et al., Quantitative and kinetic evolution of wound healing through image analysis., IEEE Trans Med Imaging 19(7) (2000) 767-772.

[14]   G. L. Hansen, et al., Wound status evaluation using color image processing, IEEE Trans Med Imaging 16 (1997) 78-86.

[15]   J. Liu, et al. Acomparative study of textures measures for human skin treatment. in Proceedings of International Conference on Information, Communication Signal Processing ICICS. 1997. Beijing, China.

[16]   C. Ribeiro, C. Barrias, and M. Barbosa, Calcium phosphate-alginate microspheres as enzyme delivery matrices, Biomaterials 25(18) (2004) 4363-4373.

[17]   M. Agren, Four alginate dressings in the treatment of partial thickness wounds: a comparative experimental study, British Journal of Plastic Surgery 49 (1996) 129-134.

[18]   G. Winter, Formation of the scab and the rate of epithelialization of superficial wounds in the skin of the young domestic pig, Nature 193 (1962) 293-294.

[19]   C. Knill, et al., Alginate fibres modified with unhydrolysed and hydrolysed chitosans for wound dressings, Polymers 55 (2004) 65-76.

[20]   S. Blair, et al., Clinical trial of calcium alginate haemostatic swabs, British Journal of Plastic Surgery 77 (1990) 568-570.

[21]   G. M. Manaker, Wound Dressing in the new Millennium, Seminars in Cutaneous Medicine and Surgery 21(2) (2002) 171-175.

[22]   I. T. Ozbolat, et al., Feature Based Bio-Modeling of Micro-patterned Structures for Tissue Engineering, Computer-Aided Design and Applications 6(5) (2009) 661-671.

[23]   Q. Sun, et al., Sustained Release of Multiple Growth Factors from Injectable Polymeric System as a Novel Therapeutic Approach Towards Angiogenesis, Pharmaceutical Research 27(2) (2010) 267-271.

[24]   S. D. Putney and P. A. Burke, Improve protein therapeutics with sustained release formulations, Nature Biotecnol. 16 (1998) 153-157.

[25] D. J. Geer, D. D. Swartz, and S. T. Andreadis, Biomimetic Delivery of Keratinocyte Growth Factor upon Cellular Demand for Accelerated Wound Healing in Vitro and in Vivo, American Journal of Pathology 167(6) (2005) 1575-1588.

[26] S. R. S. Peppe, et al., Adenovirus-mediated VEGF(165) gene transfer enhances wound healing by promoting angiogenesis in CD1 diabetic mice, Gene Ther. 9 (2002) 1271–1277.

[27] D. MacKay and A. L. Miller, Nutritional Support for Wound Healing, Alternative Medicine Review 8(4) (2003) 359-377.

[28] K. A. Choate and P. A. Khavari, Direct cutaneous gene delivery in a human genetic disease, Hum. Gene. Ter. 8 (1997) 201-211.

[29] W. R. Gombotz and D. K. Pettit, Biodegredable Polymer for Protein and Peptite Drug Delivery Bioconjugate Chemistry 6 (1995) 332-351.

[30] I. T. Ozbolat and B. Koc, Modeling of Spatially Controlled Bio-molecules in Three-dimensional Porous Alginate Structures ASME transactions, Journal of Medical Devices 4(4) (2010) 041003(1)-041003(11).

[31] RobertMcNeel&Associates, Rhinoceros 4.0, 2007: Seattle.

[32] I. T. Ozbolat and B. Koc, 3D Engineered Wound Scaffolds for Spatiotemporally Controlled Release Kinetics, in Industrial Engineering Research Conference2011: Reno, Neveda.

[33] L. Piegl and W. Tiller, *The NURBS Book*. 2nd ed1997, New York: Springer.

[34] S. Khalil and W. Sun, Biopolymer deposition for freeform fabrication of hydrogel tissue constructs, Material Science and Engineering: C 27(3) (2007) 469-478.

[35] E. Sachlos and J. T. Czernuszka, Making Tissue Engineering Scaffolds Work: Review on the application of solid freeform fabrication technology to the production of tissue engineering scaffolds, European Cells and Materials 5 (2003) 29-40.

[36] R. Chang, J. Nam, and W. Sun, Computer-Aided Design, Modeling, and Freeform Fabrication of 3D Tissue Constructs for Drug Metabolism Studies, Computer-Aided Design and Application 5 (2008) 21-29.

[37]   R. Chang, J. Nam, and W. Sun, Direct Cell Writing of 3D Micro-organ for In Vitro
       Pharmacokinetic Model, Tissue Engineering 14(2) (2008) 157-169.

[38]   B. Amsden, Solute Diffusion within Hydrogels. Mechanisms and Models, Macromolecules
       31(23) (1998) 8382-8395.

[39]   M. Grassi and G. Grassi, Mathematical Modeling and Controlled Drug Delivery: Matrix Systems,
       Controlled Drug Delivery 2 (2005) 97-116.

[40]   A. R. Kulkarni, K. S. Soppimath, and T. M. Aminabhavi, Controlled release of diclofenac sodium
       from sodium alginate beads crosslinked with glutaraldehyde, Pharmaceutica Acta Helvetiae 74
       (1999) 29-36.

[41]   S. Khalil, Deposition and Structural Formation of 3D Alginate Tissue Scaffold, in Mechaical
       Engineering Department2005, Drexel University: PA.

[42]   A. D. Polyanin, *Handbook of Linear Partial Differential Equations for Engineers and Scientists*
       2001, Bovs Raton: Chapman&Hall/CRC.

[43]   B. Albouy, Y. Lucas, and S. Treuillet, 3d Modeling from uncalibrated color images for a
       complete wound assessment tool, in Proceedings of the 29th Annual International Conference of
       the IEEE EMBS Cité Internationale2007: Lyon, France

[44]   S. A. Burns, et al., Determining the protein drug release characteristics and cell adhesion to a
       PLLA or PLGA biodegradable polymer membrane, Journal of Biomedical Materials Research
       Part A 94A(1) (2010) 27-37.

[45]   A. Khoda, I. Ozbolat, and B. Koc, Engineered Tissue Scaffolds with Variational Porous
       Architecture, ASME Transcations, Journal of Biomechanical Engineering 133(1) (2011)
       011001(1)-011001(12).

[46]   C. R. Kahn, et al., *Joslin's Diabetes Mellitus*. 14th ed2004: Lippincott Williams & Wilkins.

[47]   M. R. Rasmussen, T. Snabe, and L. H. Pedersen, Numerical modelling of insulin and
       amyloglucosidase release from swelling Ca-alginate beads, journal of Controlled Release 91(3)
       (2003) 395-405.

[48] C. Lin and A. Metters, Hydrogels in controlled release formulations: Network design and mathematical modeling, Advanced Drug Delivery Reviews 58 (2006) 1379-1408.

[49] A. S. Hickey and N. A. Peppas, Mesh size and diffusive characteristics of semicrystalline poly(vinyl alcohol) membranes prepared by freezing/thawing techniques, Journal of Membrane Science 107(3) (1995) 229-237.

[50] L. Branno-Peppas, Drug delivery systems : Vascant V. Ranade and Mannfred A. Hollinger CRC Press, Boca Raton, Florida, 1995, 364 pp. Dr Lisa Brannon-Peppas, Biomaterials 18(5) (1997) 449-449.

[51] P. L. Ritger and N. A. Peppas, A simple equation for description of solute release II. Fickian and anomalous release from swellable devices, journal of Controlled Release 5(1) (1987) 37-42.

[52] J. L. Stringer and N. A. Peppas, Diffusion of small molecular weight drugs in radiation-crosslinked poly(ethylene oxide) hydrogels, journal of Controlled Release 42(2) (1996) 195-202.

[53] N. A. Peppas, Devices based on intelligent biopolymers for oral protein delivery, International Journal of Pharmaceutics 277(1-2) (2004) 11-17.

[54] N. A. Peppas and L. Brannon-Peppas, Drug Delivery Biomaterials, in Encyclopedia of Materials: Science and Technology, eds. Editors, pp. 2351-2355(Elsevier, Oxford, 2001).

[55] C. L. Bell and N. A. Peppas, Water, solute and protein diffusion in physiologically responsive hydrogels of poly(methacrylic acid-g-ethylene glycol), Biomaterials 17(12) (1996) 1203-1218.

[56] S. W. Kim, Y. H. Bae, and T. Okano, Hyogels: Swelling, Drug Loading, and Release, 9(3) (1992) 283-2390.

Tables

Table 1: Characterization of diffusion coefficient at different alginate concentrations

Alginate Concentration (%)	M_a/M_b (Slab)	M_a/M_b (filament)	$p_{polymer}$ (g/mL)	$p_{solvent}$ (g/mL)	Q
1	73	16.576	1.01	1	0.060
1.5	56	13.750	1.015	1	0.072
2	42	11.209	1.02	1	0.088
3	30	8.795	1.03	1	0.111

Figures

Figure 1: Morphing process: (a) lofted surface generation and (b) construction of lofted volume.

Figure 2: (a) A chronic wound image [43] from the literature is processed (b) using ImageJ software and

(c) 3D NURBS surface is obtained in Rhinoceros.

a

x
y

s

b

Wound Bed Surface

Lofted
Surface
$\mathbf{S}=\{S_k(u,v)\}_{k=1,\ldots,K}$

c

Porous layer

Layer by Layer
Manufacturing

d

Region 1
Region 2
Region 3
Region 4

Functionally
Graded Regions
$\mathbf{R}=\{R_n\}_{n=1,\ldots,N}$
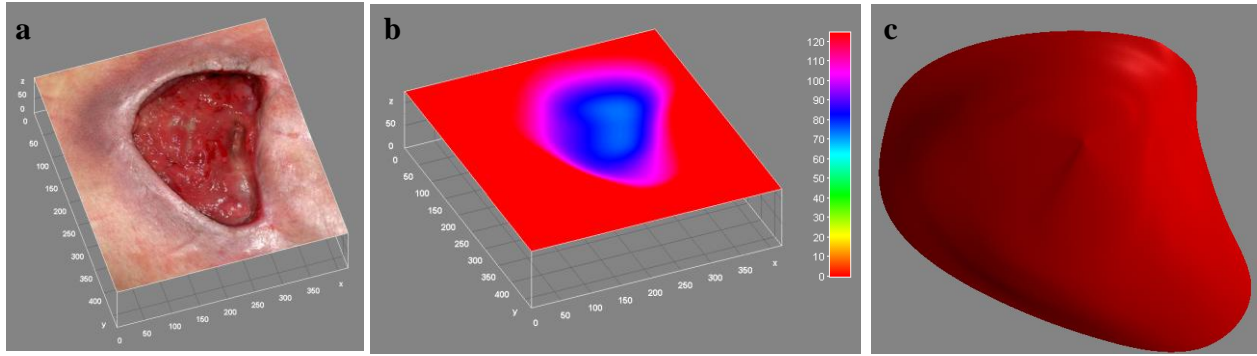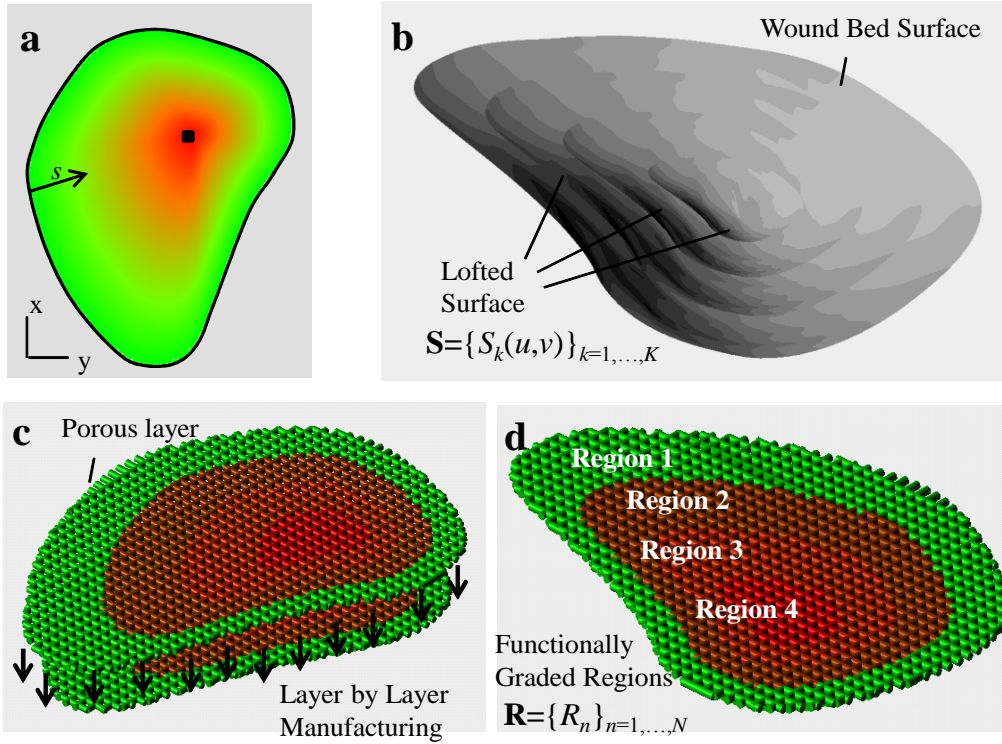
Figure 3: (a) Linear wound healing fashion from wound bed surface to final healing point, (b) generation

of lofted surface, and (c) a 3D hybrid wound device with functionally graded regions.
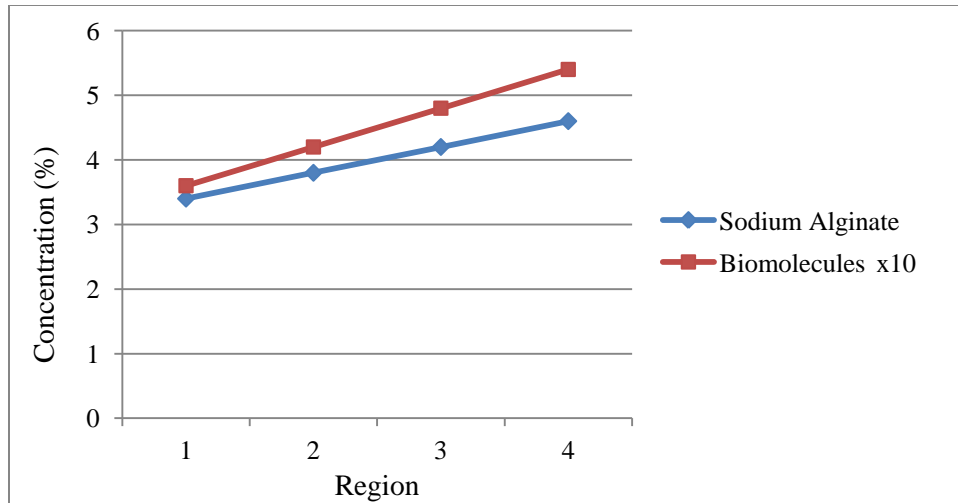
Figure 4: Concentration of sodium alginate and biomolecules
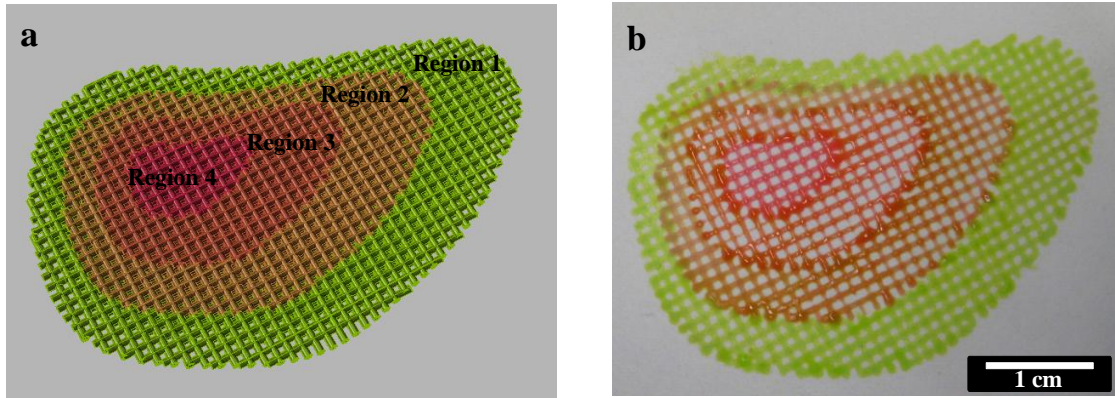
Figure 5: (a) Designed model in CAD and (b) fabricated wound device using multi-chamber single nozzle deposition system through 250µm nozzle tip.
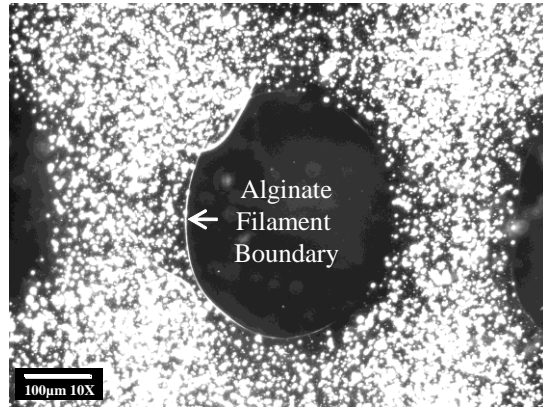
Figure 6: Dark field image of encapsulated modifiers (beads) with a uniform size distribution of 3-15 µm using 5.0x1.0x1.0 optic lenses.
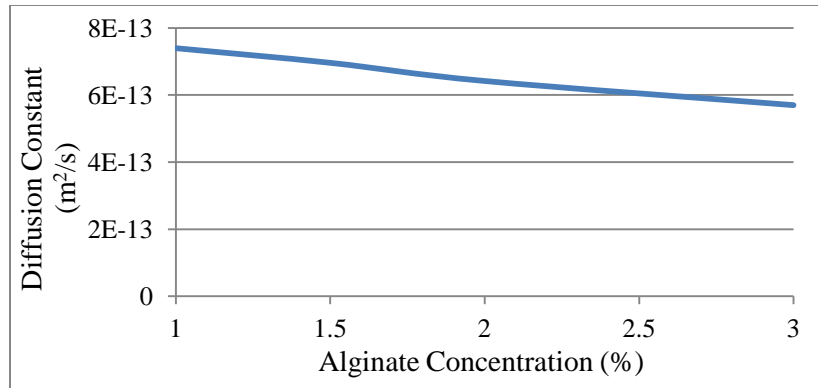
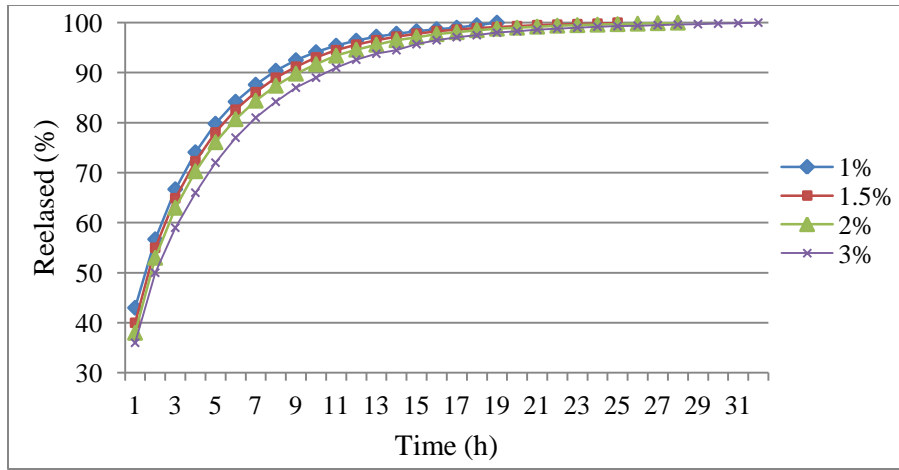Figure 7: Diffusion coefficient of insulin through alginate network at different concentrations

Figure 8: Insulin release through 250μm diameter micro-filaments for 4 different alginate concentrations

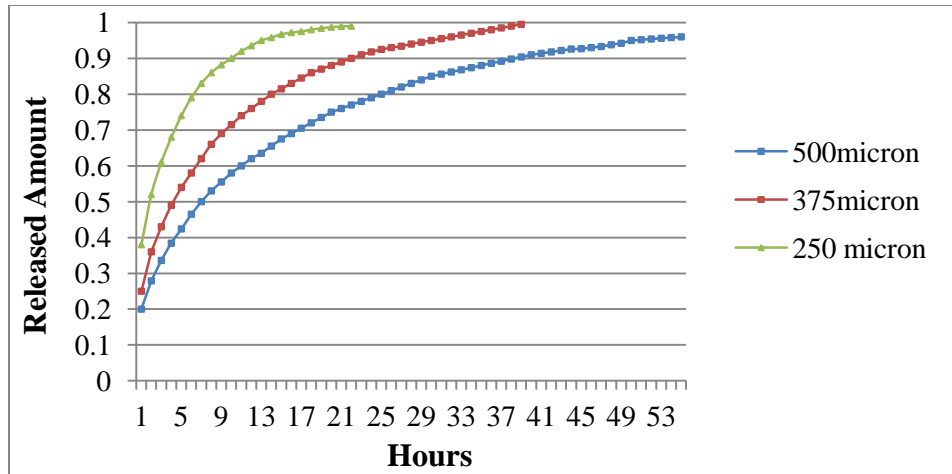Figure 9: Insulin release through 250μm, 375μm and 500μm diameter micro-filaments for 2.5% alginate concentration.